

DR. MARTIN WEAR (Orcid ID : 0000-0003-2208-2986)

Received Date : 14-Dec-2016

Revised Date : 18-Jan-2017

Accepted Date : 23-Jan-2017

Article type : Research Article

Thermo-kinetic analysis space expansion for cyclophilin-ligand interactions – identification of a new non-peptide inhibitor using Biacore™ T200

Martin A. Wear^{1*}, Matthew W. Nowicki¹, Elizabeth A. Blackburn¹, Iain W. McNae¹ & Malcolm D. Walkinshaw¹.

¹The Edinburgh Protein Production Facility (EPPF), Wellcome Trust Centre for Cell Biology (WTCCB), University of Edinburgh, King's Buildings, Max Born Crescent, Mayfield Road, Edinburgh, EH9 3BF, UK

*Corresponding Author: Martin A. Wear.

¹The Edinburgh Protein Production Facility (EPPF), Wellcome Trust Centre for Cell Biology (WTCCB), University of Edinburgh, King's Buildings, Max Born Crescent, Mayfield Road, Edinburgh, EH9 3BF, UK

E-mail: martin.wear@ed.ac.uk (MAW)

Running title.

New non-peptide fragment inhibitor for cyclophilin-A

Abbreviations.

CsA – Cyclosporin-A

DLS – Dynamic light scattering

EDC – 1-ethyl-3-(3-diaminopropyl) carbodiimide hydrochloride

His-CypA – His-tagged cyclophilin-A

IMAC – Immobilised metal affinity chromatography

ITC – Isothermal titration calorimetry

NHS – *N*-hydroxysuccinimide

NTA – Nitrilotriacetic acid

This article has been accepted for publication and undergone full peer review but has not been through the copyediting, typesetting, pagination and proofreading process, which may lead to differences between this version and the Version of Record. Please cite this article as doi: 10.1002/1878-0261.12201

Molecular Oncology (2017) © 2017 The Authors. Published by FEBS Press and John Wiley & Sons Ltd.

This is an open access article under the terms of the Creative Commons Attribution License, which permits use, distribution and reproduction in any medium, provided the original work is properly cited.

PAGE – Polyacrylamide gel electrophoresis

PDB – Protein data bank

RU – Response units

SPR - Surface plasmon resonance

SEC-MALS – Size-exclusion chromatography multi-angle light scattering.

TFE – 2,2,2-trifluoroethanol

Keywords.

Cyclophilin-A, surface plasmon resonance, thermodynamics, non-peptide, inhibitor

Conflicts of interest.

None

Abstract.

We have established a refined methodology for generating surface plasmon resonance sensor surfaces of recombinant his-tagged human cyclophilin-A. Our orientation-specific stabilisation approach captures his-tagged protein under “physiological conditions” (150 mM NaCl, pH 7.5) and covalently stabilises it on Ni²⁺-nitrilotriacetic acid surfaces, very briefly activated for primary amine-coupling reactions, producing very stable and active surfaces (≥ 95 % specific activity) of cyclophilin-A. Variation of protein concentration with the same contact time allows straightforward generation of variable density surfaces, with essentially no loss of activity, making the protocol easily adaptable for studying numerous interactions; from very small fragments, ~ 100 Daltons, to large protein ligands. This new method results in an increased stability and activity of the immobilised protein and allowed us to expand the thermo-kinetic analysis space, and to determine accurate and robust thermodynamic parameters for the cyclophilin-A:cyclosporin-A interaction. Furthermore, the increased sensitivity of the surface allowed identification of a new non-peptide inhibitor of cyclophilin-A, from a screen of a fragment library. This fragment, 2,3-diaminopyridine, bound specifically with a mean affinity of 248 ± 60 μ M. The X-ray structure of this 109 dalton fragment bound in the active site of cyclophilin-A was solved to a resolution of 1.25 Å (PDB: 5LUD), providing new insight into the molecular details for a potential new series of non-peptide cyclophilin-A inhibitors.

Introduction.

Over the course of the last decade surface plasmon resonance (SPR) systems, along with their control and analysis software, have become easier and simpler to operate, to such an extent that they are almost universally available in laboratories for the characterisation of bio-molecular interactions and small molecule drug-discovery/hit validation studies [1-9]. The major advantage of SPR instrumentation is that it allows the measurement of kinetic and affinity parameters *and* derivation of thermodynamic data specifically associated with complex formation and dissociation. Such thermodynamic profiling [10-12] can greatly enhance the correlation of solution binding measurements with structural features. This, in turn, allows the assignment of proportional energetic contributions to

individual functional groups involved in the formation of a complex; the whole basis of structure-based approaches to engineered therapeutics and drug design [9, 13-15]. The ready availability and ease of use of the technology has to be tempered with a vigorous approach to validation of the surface being studied, especially for non-experts. It is comparatively straightforward to produce an “active” sensor surface that displays a “binding response”. However, in many SPR studies the experimental design lacks appropriate optimisation, and the data generated often inappropriately interpreted and/or analysed [16-19]. This unfortunately leads to the derivation of affinity and kinetic parameters that are not physiologically appropriate to the protein/system being studied, and poor correlation with the literature data from alternative approaches.

We have developed a simple and refined methodology for generating highly stable and active SPR sensor surfaces of recombinant human his-tagged cyclophilin-A (His-CypA). Surfaces created by this approach produce values for the kinetic, equilibrium and thermodynamic parameters for the binary cyclophilin-A:cyclosporin-A (CsA) complex that correlate extremely well with data determined by a multitude of other solution techniques [20-30]. Cyclophilins are a large subfamily of isomerases that catalyse the conversion of prolyl-cis/trans isomers in folding polypeptide chains (PPIases, EC. 5.2.1.8). The most extensively studied member of the family is the cytoplasmic isoform CypA and its natural, low-nanomolar affinity, immunosuppressive cyclic undecapeptide inhibitor cyclosporin A (CsA) [31]. As well as playing roles in protein folding, CypA appears to be a fundamental component in numerous quite disparate biological processes [32] including viral infections [33-41], responses to inflammation [42] and a growing number of proliferative cancers and malignancies [43-45]. This has resulted in considerable interest in the development of non-immunosuppressive, non-peptide CypA inhibitors as mechanistic tools and potential drugs for various diseases.

Although the basic framework of the methodology described in this article is grounded on initial work developed in our lab, the new protocols have been very significantly, and rationally, optimised. Our orientation-specific stabilisation approach captures his-tagged proteins under “physiological conditions” (150 mM NaCl, pH 7.5) on Ni²⁺-charged nitrilotriacetic acid (NTA) surfaces, which have been very briefly activated for primary amine-coupling reactions. This produces very stable and active surfaces of His-CypA. Simple alteration of protein concentration with the same contact time (30 sec) allows variable density surfaces to be easily made, with no loss of specific activity. Surfaces can thus be easily tailored for the study of numerous interactions; ranging from very small fragments (~ 100 daltons) through to large protein ligands. The streamlined procedure increased the stability and activity of the protein on the sensor surfaces and allowed us to greatly expand the thermo-kinetic analysis space; from 5 °C to 44 °C. We subsequently generated much more detailed and robust sets of kinetic and thermodynamic parameters for the CypA:CsA interaction and identified and characterised a small fragment, 2,3-diaminopyridine (Mw = 109 Da.) that bound stoichiometrically to the active site of His-CypA with a mean K_d of $248 \pm 60 \mu\text{M}$. The X-ray structure of this fragment bound in the active site of CypA was also solved to a resolution of 1.25 Å (PDB: 5LUD), providing new insight into the molecular details for potential development of a new series of non-peptide CypA inhibitors.

Materials and Methods.

Materials. All chemicals used were of the highest grade available commercially.

Plasmid construction, protein production and purification. The open reading frame encoding for full length human CypA (M1 – E165) was synthesized and codon optimized (GENEART) for expression in *E. coli*, with a hexahis tag (underlined), linker and a TEV protease cleavage site (bold, underlined) fused to the N-terminus (MSKYHHHHHDYDIPTTENLYFQ/G-M1-CypA). Standard GATEWAY® methodology was used to generate an expression vector in pDEST™14 (ThermoFisher). Recombinant protein was over-expressed and purified to homogeneity from OverExpress C41 BL21(DE3) *E. coli* (Lucigen), grown shaking (260 rpm) at 30 °C for 16 hrs in 50 mls of EnPresso media (BioSilta) containing carbenicillin (100 µg.ml⁻¹). Cell pellets were resuspended in 20 mM NaH₂PO₄, pH 7.4; 500 mM NaCl; 20 mM imidazole; plus protease inhibitors at 10% wt/vol, and lysed at 6 °C by a single passage through a Constant Systems Cell Disruptor (1.1 kW TS Benchtop) set at 22 kpsi, followed by centrifugation at 50,000 xg for 1 hr at 4 °C. The supernatant was filtered (0.22 µm) and then subsequently loaded onto an ÄKTAXpress™ (GE Healthcare) system fitted with 5 ml HiTrap Ni²⁺-IMAC FF (GE Healthcare) and HiPrep S200 26/60 HR (GE Healthcare) columns, with standard configuration and settings for a 2-step affinity-gel-filtration protocol. A single 10-column volume step to 100% *IMAC Elution buffer* was used for elution from the IMAC column. Buffers used for the purification were; *IMAC Loading buffer*: 20 mM NaH₂PO₄, pH 7.4; 500 mM NaCl; 20 mM Imidazole; 100 µM PMSF. *IMAC Elution buffer*: 20 mM NaH₂PO₄, pH 7.4; 500 mM NaCl; 500 mM Imidazole. *Gel-Filtration Buffer*: 10 mM NaH₂PO₄, pH 7.5; 150 mM NaCl; 50 µM EDTA. His-CypA was concentrated to 100 µM and stored at 4 °C in *Gel-Filtration Buffer* or processed for X-ray crystallography (see below). The standard culture and purification conditions described above result in a final yield of 19.8 mg, per litre equivalent, of ≥ 95% pure (judged by SDS-PAGE) His-CypA.

Mono-dispersity and size analysis. Size-exclusion chromatography (ÄKTAMicro™, GE Healthcare) coupled to UV, static light scattering and refractive index detection (Viscotek SEC-MALS 20 and Viscotek RI Detector VE3580; Malvern Instruments) were used to determine the absolute molecular mass of His-CypA in solution. Multiple injections of 100 µL of 1 mg·ml⁻¹ (47.5 µM) His-CypA were run on a calibrated Superdex-75 10/300 GL (GE Healthcare) size exclusion column pre-equilibrated in 10 mM NaH₂PO₄, pH 7.5; 150 mM NaCl; 50 µM EDTA at 22 °C with a flow rate of 0.8 ml·min⁻¹. Light scattering, refractive index (RI) and A_{280nm} were analysed by a homo-polymer model (OmniSEC software, v5.02; Malvern Instruments) using the following parameters for His-CypA: $\partial A_{280nm} / \partial c = 0.71 \text{ AU}\cdot\text{ml}\cdot\text{mg}^{-1}$, $\partial n / \partial c = 0.185 \text{ ml}\cdot\text{g}^{-1}$ and buffer RI value of 1.334. Mass distribution analysis of the pure His-CypA protein solutions by dynamic light scattering (DLS) was performed on a Zetasizer APS (Malvern Instruments) with 5 repeat runs of 60 µl (1 mg·ml⁻¹) in 10 mM NaH₂PO₄, pH 7.5; 150 mM NaCl; 50 µM EDTA, at 22 °C, with a 120 s equilibration.

Peptidyl prolyl isomerase (PPIase) assay. This assay determines the rate of the *cis* to *trans* conversion of the peptidyl-prolyl amide bond in the substrate *N*-succinyl-Ala-Ala-Pro-Phe-*p*-nitroanilide (AAPF-pNA). Selective hydrolysis of AA*trans*PF-pNA by α -chymotrypsin releases *p*-nitroaniline, the accumulation of which is monitored by absorbance at 400 nm. AAPF-pNA, in 470 mM LiCl; 2,2,2-trifluoroethanol (TFE) at 200 mM, was diluted to 4 mM in the same buffer immediately before use. Reactions were conducted at 12 °C on a Jasco V550 spectrophotometer with temperature control, in 50 mM HEPES, pH 8.0; 100 mM NaCl; 0.5 mM DTT, in a total volume of 1 ml, essentially as described [26, 28] with minor modifications. The final concentration of His-CypA and AAPF-pNA were 12.3 nM and 100 μ M, respectively. The apparent equilibrium dissociation constant, K_{iapp} , for the inhibitor was determined by a least squares fit of equation 1 to plots of the initial reaction rate (background thermal isomerisation rate subtracted), V_o (in μ M.s⁻¹) versus the concentration of CsA in nM.

$$V_o = (V_i / 2 \times [hCypA] \times \{([hCypA] - [CsA] - K_{iapp}) + \sqrt{([hCypA] - [CsA] - K_{iapp})^2 + (4 \times [hCypA] \times K_{iapp})}\})$$

Equation 1.

Where V_i is the reaction rate at zero inhibitor concentration, $[CsA]$ is the concentration of added CsA, K_{iapp} is the apparent equilibrium dissociation constant of CsA and $[hCypA]$ is the concentration of His-CypA. Correction for competition with sAA*cis*PF-pNA substrate was performed using equation 2.

$$K_d = K_{iapp} / 1 + ([Sub] / K_m)$$

Equation 2

where $[Sub]$ is the initial AA*cis*PF-pNA concentration (mean concentration = $54.7 \pm 2.9 \mu$ M, \pm SE, $n = 9$) and K_m is the Michealis constant of the substrate. For His-CypA the mean (\pm SE, $n = 9$) K_m , k_{cat} and k_{cat}/K_m values are $703 \pm 72 \mu$ M, $6,134 \pm 233 \text{ s}^{-1}$ and $8.06 \times 10^6 \text{ M}^{-1} \cdot \text{s}^{-1}$, respectively.

Surface plasmon resonance (SPR) equipment and reagents. SPR measurements were performed using a BIAcore T200 instrument (GE Healthcare). Ni²⁺-nitrilotriacetic acid (NTA) and CM5 sensor chips, 1-ethyl-3-(3-diaminopropyl) carbodiimide hydrochloride (EDC), *N*-hydroxysuccinimide (NHS) and ethanolamine (H₂N(CH₂)₂OH) were purchased from GE Healthcare.

Optimised capture/stabilization of His-CypA. Pure His-CypA was immobilized and covalently stabilised on an NTA sensor chip using a refined protocol to that initially described [25]. Following Ni²⁺ priming (30 sec injection of 500 μ M NiCl₂ at 5 μ l·min⁻¹), dextran surface carboxylate groups were minimally activated by an injection of 0.2 M EDC; 50 mM NHS at 5 μ l·min⁻¹ for between 30 and 420 sec. His-CypA (at concentrations between 10 and 400 nM), in 10 mM NaH₂PO₄, pH 7.5; 150 mM NaCl; 50 μ M EDTA was captured *via* the hexa-his tag and simultaneously covalently stabilised on the surface by injection for 30 seconds, at 30 μ l·min⁻¹. Immediately following the capture/stabilisation step a single 15 sec injection of 350 mM EDTA and 50 mM Imidazole in 10 mM NaH₂PO₄, pH

7.5; 150 mM NaCl; 0.05% surfactant P20, 1 % ethanol, at 30 $\mu\text{l}\cdot\text{min}^{-1}$ was used to remove non-covalently bound protein, followed by a 180 sec injection of 1 M $\text{H}_2\text{N}(\text{CH}_2)_2\text{OH}$, pH 8.5 at 5 $\mu\text{l}\cdot\text{min}^{-1}$. The surface was further conditioned with a 600 sec wash with 10 mM NaH_2PO_4 , pH 7.5; 150 mM NaCl; 0.05 % surfactant P20, 1 % ethanol; 1 mM EDTA at 100 $\mu\text{l}\cdot\text{min}^{-1}$. Specific protein activity was assayed by passing saturating amounts of CsA (1.0 μM) in 10 mM NaH_2PO_4 , pH 7.5, 150 mM NaCl, 50 μM EDTA; 0.05 % surfactant P20; 1 % ethanol over the surface and was invariably greater than 95 % for all densities generated.

Direct covalent immobilization of His-CypA. His-CypA was immobilized on a CM5 sensor chip utilising standard amine coupling chemistry. The sensor chip surface was activated by an injection of 0.2 M EDC; 50 mM NHS at 5 $\mu\text{l}\cdot\text{min}^{-1}$ for 420 s. His-CypA (theoretical pI = 6.54) at 100 $\mu\text{g}\cdot\text{ml}^{-1}$ in 10 mM acetate, pH 5.8, and injected over the activated surface for 30 sec. The amount of His-CypA immobilized on the activated surface was typically between 580 and 800 RU. After the immobilization of the protein, a 420 sec injection at 5 $\mu\text{l}\cdot\text{min}^{-1}$, of 1 M $\text{H}_2\text{N}(\text{CH}_2)_2\text{OH}$, pH 8.5, was used to quench excess active succinimide ester groups. The surface was further conditioned with a 600 sec wash with 10 mM NaH_2PO_4 , pH 7.5; 150 mM NaCl; 0.05 % surfactant P20, 1 % ethanol at 100 $\mu\text{l}\cdot\text{min}^{-1}$

SPR thermodynamic experiments. SPR single cycle kinetic experiments with CsA were performed, in triplicate at temperatures from 5 °C to 44 °C, in 3 °C increments. A 3-fold concentration series of CsA ranging from 2.47 nM – 200 nM, in 10 mM NaH_2PO_4 , pH 7.5, 150 mM NaCl, 1 mM EDTA; 0.05 % surfactant P20; 1 % ethanol, was injected over the sensor surface, at 100 $\mu\text{l}\cdot\text{min}^{-1}$ with 60 sec contact and dissociation times. The sensor surface was regenerated between experiments by dissociating any formed complex in running buffer for 1,800 sec at 100 $\mu\text{l}\cdot\text{min}^{-1}$. The apparent on-rate, off-rate and equilibrium dissociation constants were calculated from the sensorgrams by global fitting of a 1:1 binding model, with mass transport considerations, using analysis software (v2.02) provided with the Biacore T200 instrument.

Thermodynamic calculations. For equilibrium thermodynamics, the van't Hoff equation states:

$$\ln K_d = (\Delta H^\circ / RT) - (\Delta S^\circ / R) \quad \text{Equation 3}$$

where K_d is the equilibrium dissociation constant, R is the universal gas constant, T is the absolute temperature (K), ΔH° is the standard enthalpy change and ΔS° is the standard entropy change. Plots of $\ln K_d$ versus $1 / T$ should be a straight line, with a slope of $\Delta H^\circ / R$ and an intercept on the ordinate of $\Delta S^\circ / R$. However, this simplified relationship will not hold if the heat capacities of the reactants differs from the heat capacity of the complex and the relationship between $\ln K_d$ versus $1 / T$ becomes

$$RT \cdot \ln K_d = \Delta H^\circ_{T^*} - T \Delta S^\circ_{T^*} + \Delta C_p^\circ \cdot (T - T_0) - T \Delta C_p^\circ \cdot \ln(T / T_0) \quad \text{Equation 4}$$

where ΔC_p° is the heat capacity change under standard conditions, and T_0 is the reference temperature (298 K) [46].

Data was fitted using Kaleidagraph v4.1.3 software (Synergy Software, reading, PA).

Fragment library and compound screening. The Scottish Hit Discovery Facility fragment library (670 bioactive fragments) was obtained from the University of Dundee Drug Discovery unit. Compounds were initially screened at 1 mM on a surface of 2,866 RU of His-CypA (flowcell-2) and ~ 10,000 RU of covalently immobilised (using standard amine chemistry) human serum albumin (HSA; flowcell-4) in 10 mM NaH₂PO₄, pH 7.5; 150 mM NaCl; 50 μM EDTA; 0.05 % surfactant P20; 1 % DMSO, at 30 μl·min⁻¹ with a contact time of 30 sec and dissociation time of 120 sec. Solvent correction, carry-over assessment and a 25 % DMSO wash between samples were performed as standard. Cyclophilin-A-specific hits were further analysed with a 2-fold concentration series from 0.0625 mM to 1 mM in 10 mM NaH₂PO₄, pH 7.5; 150 mM NaCl; 50 μM EDTA; 0.05 % surfactant P20; 1 % DMSO, at 30 μl·min⁻¹ with a 30 sec contact and dissociation time.

Crystallisation and X-ray crystallography. The His-tag was removed from CypA by His-TEV protease (1:100 ratio, TEV:His-CypA with a 2 hr incubation at 30 °C) and the protein re-purified as above to remove free His-tag, His-TEV protease and any remaining uncleaved His-CypA. Protein was concentrated to 25 mg·ml⁻¹ in *Gel-filtration Buffer* (see above), minus EDTA, and crystals were grown by vapor diffusion using the hanging-drop method. CypA protein solution was mixed 1:1 with 100 mM Tris, pH 8.0; 22 % PEG 8000 and crystals were obtained after one day at 4 °C. CypA:2,3-diaminopyridine complex was prepared by transferring a coverslip containing a drop of native CypA crystals over a well solution of 35 % PEG 8000 and equilibrating at 4 °C for 24 h. Following this, a single CypA crystal was transferred into a 1 μl drop of 100 mM Tris, pH 8.0; 35 % PEG 8000; 100 mM 2,3-diaminopyridine, and allowed to soak for 60 seconds. The crystal (~ 0.2 mm in length) was then immediately mounted in a 0.2-mm cryo-loop (Hampton Research) and flash cooled in liquid nitrogen, with soaking solution acting as cryoprotectant. All diffraction data were collected at 100 K at the Diamond Light Source (DLS), on station I02. Data processing was carried out using MOSFLM [47] and AIMLESS [48]. The isomorphous structure of cyclophilin-A in complex with the dipeptide Gly-Pro (PDB ID 4N1M) was used to solve the structure using the program REFMAC, [49] part of the CCP4 [50] suite of programs. Refinement and model building were performed using the program COOT [51].

Data accessibility. Atomic coordinates have been deposited in the Brookhaven Protein Data Bank under the accession number PDB: 5LUD.

Miscellaneous. The molecular weights of CsA, His-CypA and 2,3-diaminopyridine are 1202.12 Da., 21,040 Da. and 109 Da., respectively. Protein concentration was determined by A₂₈₀ measurement and the extinction coefficient 14,690 M⁻¹·cm⁻¹.

Results and discussion.

One of the key criteria for successful SPR experiments is having access to very pure, mono-disperse, active and stable protein. Our lab has previously generated protocols for the production and purification of numerous cyclophilins with very high purity and specific activity, both as tagged and untagged reagents, from bacterial sources [22, 26]. We have streamlined a protocol for His-CypA purification (see material and methods) and Figure 1 shows the typical high purity ($\geq 95\%$), mono-dispersity and activity of the protein used in all our experiments. Size-exclusion chromatography multi-angle light scattering (SEC-MALS) analysis was used to determine the molecular mass and mono-dispersity of purified His-CypA in solution. On a Superdex-75 10/300 GL (GE Healthcare) size exclusion column, His-CypA protein elutes a single sharp and symmetrical peak with a correlative R_s of 1.82 ± 0.11 nm (Figure 1B). The molar mass average across the elution profile is 19.8 ± 0.4 kDa. with excellent mono-dispersity ($M_w/M_n = 1.003$). This is in excellent agreement with theoretical molecular weight of 21.04 kDa. for monomeric His-CypA. DLS (data not shown) analysis also indicates high mono-dispersity for His-CypA solutions with a mean R_h of 1.85 ± 0.17 nm (mean \pm SEM, $n = 5$), a polydispersity index of ≤ 0.1 and a correlative molecular weight of between 19 to 21 kDa, consistent with a highly pure and monomeric protein solution. This protein is also highly enzymatically active; Figure 1C shows the typical inhibition of His-CypA's PPIase activity by CsA. The mean k_{cat} value of $6,134 \pm 233$ s⁻¹ and the K_i value for CsA of 15.03 ± 1.38 nM (\pm SEM, $n = 9$) are again consistent with coherent protein with a very high specific activity [26, 28].

Covalent immobilisation of proteins *via* primary amines coupling is regularly the method of choice for generating SPR sensor surfaces with no baseline drift. It is a rapid and well-established process and simple to implement. However, a significant proportion of proteins are incompatible with such covalent coupling strategies and as a consequence have aberrant or low binding activity, or are even completely inactive, upon immobilisation. This is certainly the case for the human cyclophilins, especially CypA, in our hands [26, 52]. Alternative non-covalent capture methodologies like the His-tag: Ni^{2+} -NTA interaction, are robust and allow for repeated immobilisation, stripping, and regeneration of the surface [53]. Nevertheless, these surfaces can often have low binding capacities, and/or exhibit a slow and continuous dissociation of the immobilised protein from the surface [26, 52, 53]. Such baseline drift, particularly prevalent with high protein immobilization levels (due to loss of rebinding events) regularly required for small molecule work, can create problematic assessment of the binding kinetics. Previous work from our lab had investigated various orientation-specific capture/stabilisation methods for the immunophilins, human CypA [25, 26] and human FK506 binding protein (FKBP12) [52] that could not be actively immobilised by standard methods. Here we report on the development of a simple and streamlined methodology for His-CypA, that allows creation of very stable (in excess of 500 individual cycles without significant decay in saturating ligand concentration responses) and active SPR sensor surfaces (typically in excess of 95 % specific activity). The approach captures and orients His-tagged protein under "physiological" ionic and pH conditions (minimising or eliminating any spurious electrostatic adsorption to the dextran matrix) on NTA surfaces previously charged with Ni^{2+} and *minimally* activated for primary amine-coupling reactions, prior to protein contact.

We first determined the length of time the sensor surfaces were activated prior to his-tagged protein capture

was important for not only the final level of protein immobilisation, but also critically the specific activity of the captured/stabilised molecules. The optimal time for EDC:NHS activation of the pre-charged Ni²⁺-NTA sensor surface was invariably between 150 seconds and 240 seconds, regardless of the concentration of protein used (Figure 2A). Less than 150 seconds of activation time resulted in low and more variable levels of stabilised protein on the surface (Figure 2A). Activating for longer than 240 seconds resulted in the specific activity dropping markedly below 80 % (Figure 2A) and the resultant binding parameters measured using such surfaces for the CypA:CsA interaction deviate markedly from accepted values for these constants. In our hands, neither the kinetics of binding, nor the specific activity of the surface, were affected to any significant extent by the amount of protein immobilised on the surface. Simply changing the concentration of His-CypA from 10 nM to 400 nM, whilst keeping the divalent charging (30 sec), activation (180 sec), protein contact (30 sec for all densities) and quenching (180 sec) to minimal constant times, allowed us to both standardise the method and generate sensor surfaces with between ~ 50 RU and ~ 4,000 RU of stabilised protein. Typical sensorgrams, monitored on intermediate (~ 600 RU) and extremely low (~ 50 RU) density surfaces of covalently stabilised His-CypA binding to CsA, are shown in Figure 2B & C. The on-rate (k_+), off-rate (k_-) and equilibrium dissociation constants (K_d) are essentially identical for both surfaces. Mean values for k_+ , k_- and K_d at 25°C, on intermediate density surfaces are $0.79 \pm 0.06 \mu\text{M}^{-1}\cdot\text{s}^{-1}$, $0.018 \pm 0.004 \text{ s}^{-1}$ and $22.8 \pm 3.6 \text{ nM}$ (Figure 2B), respectively, compared to $0.73 \pm 0.07 \mu\text{M}^{-1}\cdot\text{s}^{-1}$, $0.018 \pm 0.006 \text{ s}^{-1}$ and $24.7 \pm 5.3 \text{ nM}$ (Figure 2C), on low density surfaces. Our data here is in excellent agreement with the values for these biophysical parameters determined in solution studies by ITC [20, 24, 25], fluorescence titration [23, 25-27, 29], SPR [25, 26], enzymatic analysis [23, 26, 28, 29] and NMR [21].

Capture *via* the His-tag, under “physiological” pH and salt concentration, reduces or eliminates any electrostatic adsorption to carboxymethyl dextran matrix, whilst orienting the protein away from the sensor surface, and prevents any uncontrolled and spurious coupling reactions that are liable to compromise the coherency of the immobilised protein. The covalent reaction on these surfaces is therefore focused and brief, and only occurs proximally to the His-tag; likely either the N-terminus itself or the lysine residue N-terminal to the hexa-his sequence in the construct. Similar rationales have been used for making sensor surfaces with whole cellular receptors [54] and His-RGS proteins [55]. In our hands, standard covalent coupling methods have never yielded satisfactory results for the cyclophilins. As previously discussed [26], the X-ray structure of CypA [56] shows the majority of surface exposed lysine residues are located on the CsA-binding face of the molecule giving it a predominantly basic character. Under the acidic solution conditions (even mildly acidic) required for the standard primary amine immobilisation process, the surface charge potential of CypA seems likely to force the molecule to orient with the CsA-binding surface face-down on the matrix, resulting in severe steric occlusion of this site for ligand access. A further consideration that contributes to low protein activity when using direct coupling approaches is an acidic pH-shift-dependent affinity loss that occurs quite rapidly with CypA. This behavior has been observed in ITC, intrinsic fluorescence experiments with CypA and its ligands [26, 30, 57]. The reasons and mechanism for this are not entirely clear, but it involves a combination of protein protonation and a resultant partial irreversible denaturation of the protein in solutions with a pH below ~ 5.5 that leads quickly to irreversible structural changes and aberrant binding behaviour [26, 30, 57].

The most effective conditions we have found in our laboratory so far for direct coupling of CypA are 100 - 120 $\mu\text{g}\cdot\text{ml}^{-1}$ protein in 10 mM acetate buffer, pH 5.8 (the predicted pI of the protein is 6.54), with a 30 second contact time on an activated CM5 sensor surface. Figure 2D illustrates the type of data typically generated from such surfaces. The protein immobilised on these sensors is very clearly compromised in terms of its biophysical state. Longer contact times reduce the already poor specific activity and anomalous ligand binding behavior further. The specific activity is only around 35 % and it decays quite rapidly. Furthermore, the interaction is clearly not 1:1 and has ill-defined multiphasic kinetics (Figure 2D). The mean values (mean \pm SEM, n = 3) for k_a , k_d and K_d , at 25 $^{\circ}\text{C}$, determined from fitting a 1:1 model, for which the data is clearly not well described, are $0.48 \pm 0.1 \mu\text{M}^{-1}\cdot\text{s}^{-1}$, $0.14 \pm 0.1 \text{ s}^{-1}$ and $291.7 \pm 104 \text{ nM}$, respectively. The affinity is 12- to 14-fold weaker with significantly altered kinetics; k_d is 8- to 10-fold faster and the k_a 2-fold slower, compared to the interaction assessed on surfaces of oriented and stabilised His-CypA (compare Figure 2B and D). This very clearly indicates that this is a protein surface that is far from being biophysically coherent and does not agree with the data from other solution studies. The accepted K_d range for the CypA:CsA interaction sits between 10 – 30 nM, with the variation arising from slight differences in the buffer systems and their ionic strength, the pH, the temperature of analysis, and the specific analysis technique used in the particular study in question [20, 21, 23-30]. Surfaces of CypA generated by direct covalent immobilisation should really not then be utilised in any further experiments as they lack any rigorous correlative validation from any orthogonal techniques. Regrettably for the cyclophilins, and especially CypA, there are repeated examples in the literature where SPR sensor surfaces, all generated by standard primary amine coupling chemistry and showing very inappropriate and non-native affinities and kinetics, have been used to screen/assay ligands. There are instances where such surfaces have been used without *any* assessment of appropriate activity with a positive control, others where surfaces are used despite the affinity for CsA being reported as being orders of magnitude weaker (10- to 50-fold) than the normal expected range, and others still where the apparent binding affinities of ligands assessed by SPR do not correlate at all with any other assays employed in the study [58-61]. This is poor practice and at best, muddies the water for the field.

We next assessed the ability of our His-CypA surfaces to produce equilibrium thermodynamic data. Our streamlined surface generation clearly increased the coherency and stability of the protein on the sensor surfaces, allowing for a significant expansion of the thermo-kinetic analysis space from 5 $^{\circ}\text{C}$ to 44 $^{\circ}\text{C}$, compared to the previous range of ~ 16 $^{\circ}\text{C}$ to ~ 35 $^{\circ}\text{C}$ [25, 26]. The protein on these new surfaces was stable at temperatures up to 44 $^{\circ}\text{C}$ and could be repeatedly raised to this temperature without significant loss of binding activity or deviation in the kinetics. Single cycle kinetic experiments with CsA were performed at temperatures ranging from 5 $^{\circ}\text{C}$ to 44 $^{\circ}\text{C}$, in 3 $^{\circ}\text{C}$ increments, with a 3-fold dilution series of CsA from 2.45 nM to 200 nM. Figure 3 shows typical fitted data from a high-density sensor surface and the k_a , k_d and K_d values derived from this analysis shown in Table 1. This increased sensor surface stability permits analysis of ligand interactions at physiologically relevant temperatures, critical for proper exploration of the temperature effects on the affinity and kinetics in small molecule drug-discovery studies. Additionally, the increased sensitivity and structural integrity of the protein surface also allowed us to routinely use lower concentrations of CsA, eliminating the solubility issues with CsA (a very hydrophobic molecule), and allowing extension by over 10 $^{\circ}\text{C}$ of the lower temperature analysis range.

From 5 °C to 44 °C, the off-rate for CsA is increased ~ 175-fold compared to a ~ 9-fold increase in the on-rate (Table 1), resulting in a 23-fold loss of affinity from ~ 5 to ~ 120 nM (Figure 4A, Table 1). The van't Hoff plot of this data is very clearly non-linear (Figure 4) indicating a change in the heat capacity (ΔC_p) of the system upon binding. A fit of Equation 4 to this data (solid line, Figure 4) gives the following thermodynamic parameters at standard temperature (25 °C); $\Delta G^\circ = -10.38 \pm 0.21 \text{ kcal}\cdot\text{mol}^{-1}$, $\Delta H^\circ = -15.50 \pm 0.8 \text{ kcal}\cdot\text{mol}^{-1}$, $T\Delta S^\circ = -5.12 \pm 0.5 \text{ kcal}\cdot\text{mol}^{-1}$; $\Delta C_p = -0.41 \pm 0.16 \text{ kcal}\cdot\text{mol}^{-1}\cdot\text{K}^{-1}$ (Table 1). Negative ΔC_p values can be correlated to reduced solvent accessibility for non-polar surfaces during complex formation. They are often also indicative of conformational complexity in one or other of the components of the reaction, with changes in conformation between free and complexed states being markedly different. Another important contributor to negative ΔC_p values is the trapping of water molecules at the binding interface of the complex, often forming or contributing to a critical feature of the binding interaction surface, with each water having been calculated to contribute about $-0.05 \text{ kcal}\cdot\text{mol}^{-1}\cdot\text{K}^{-1}$ to the overall ΔC_p [57, 62]). The heavily enthalpic CypA:CsA interaction is primarily driven by hydrophobic and van der Waals interactions, but also critically, contacts that involve 5 well defined water molecules trapped at the binary complex interface [57, 62]. This coupled to the significant entropic cost of complexing a large and flexible ligand such as CsA (a cyclic undecapeptide [63]), explains the energetic parameters and the very obvious negative ΔC_p in relation to the CypA:CsA complex structure [25, 57, 62-65].

The thermodynamic parameters determined here agree exceptionally well with those measured in Fanghänel *et al*'s detailed study of the CypA:CsA interaction by ITC, performed at 25 °C in 25 mM phosphate buffer at pH 7.5; $\Delta G^\circ = -10.69 \pm 0.11 \text{ kcal}\cdot\text{mol}^{-1}$, $\Delta H^\circ = -14.7 \pm 0.03 \text{ kcal}\cdot\text{mol}^{-1}$, $T\Delta S^\circ = -3.8 \text{ kcal}\cdot\text{mol}^{-1}$; $\Delta C_p = -0.44 \pm 0.007 \text{ kcal}\cdot\text{mol}^{-1}\cdot\text{K}^{-1}$ [57]. The very small disparities arise due to subtle differences in the analysis platforms and varying contributions from solvation/desolvation effects, buffer ionization/proton exchange effects (although essentially eliminated at pH 7.5) and conformational fluctuations (free diffusion *versus* surface immobilized) in the reactants during complex formation. There is now excellent convergence in the ΔC_p values determined from this SPR study, those determined from rigorous ITC analysis [57] and those calculated from structure based calculations on the CypA:CsA binary complex; all are essentially $\sim 0.4 \text{ kcal}\cdot\text{mol}^{-1}\cdot\text{K}^{-1}$ [25, 57, 62-65]. The agreement with solution, and label free studies, further supports the view that our His-CypA SPR sensor surfaces, and the interaction of ligands with the protein, are unaffected by the immobilisation process and behave essentially as they would if free in solution and are representative of the correct physiological interaction. 1000 RU of CypA on the surface corresponds to $\sim 3 \times 10^{10}$ protein molecules immobilised within a volume of $\sim 1 \times 10^{14} \text{ nm}^3$. This gives an average intermolecular spacing between each His-CypA molecule of at least 120 Å. 2000 RU gives spacing of ~ 85 Å and 3000 RU ~ 50 Å. None of these densities would have surface "crowding" issues, and little possibility of heterogeneity arising due to steric occlusion by neighbouring molecules. This sparse and stable binding arrangement goes partway to explaining the excellent agreement in the values for the kinetic and equilibrium constants from our SPR data, the other solution techniques.

The BIAcore T200 instrument used in this study is by far the best platform for analysing such a system, both in terms of the signal-to-noise limits (baseline noise limits are $< 0.03 \text{ RU}$ (RMS), $< 0.1 \text{ (RMS)}$ and $< 0.33 \text{ RU}$ (RMS) for the T200, T100 and 3000 systems, respectively; sourced directly from GE Healthcare product technical

specification data) and the temperature control for analysis. A note here; the new BIAcore S200 system has better specifications for baseline noise, < 0.0015 RU (RMS), but with the same sensitivity for ligand detection as the T200, but we do not have access to, nor have we tested the system.

The T200 system has an operating temperature range of 4 – 45 °C, and will actually achieve the limits of this range. The T100 has the same stated range limits, but this is heavily dependent on the ambient temperature the instrument the system is operated in. We know from experience the system was able to only practically cool to ~ 18 °C below ambient under standard laboratory conditions (even though the stated maximum is 20 °C). The 3000 instrument possesses a manufacturers quoted range of 4 – 40 °C (less than the other two systems at the top end by 5 °C). Again, this is even more dependent on the ambient operating temperature the instrument the system is operated in. Our experience is that this system is able to only practically cool to ~ 15 - 16 °C below ambient (even though the stated maximum is 20 °C, this can only really be achieved reliably in environments with ambient temperatures of 18 – 19 °C). The superior functionality and sensitivity of the BIAcore T200 and the significantly increased activity and stability of the protein surfaces were primary factors in our ability to extend the thermo-kinetic analysis space reliably.

The thermodynamic parameters generated across this expanded range by this new method are much more comprehensive and robust, and there is now a very good convergence in the energetic parameters for binding CsA, particularly for the ΔC_p parameter, between the results reported here and those determined by ITC and structure based calculations [57, 63], where buffer systems have been matched. Notably, ΔC_p is notoriously difficult to determine by non-calorimetric methods and a critical factor in formulating a complete understanding and rationalization of the binding interface and structural features driving molecular recognition/complex formation; vital for rational ligand/drug design. This is especially so when using atomic resolution structures to guide the development of new ligands.

It is also noteworthy that the buffer system used here is phosphate buffered saline compared to HEPES buffered saline used previously. The thermodynamic parameters that have been determined by our lab and others change dependent on the buffer system used in the analysis. The changes can be small and sometime subtle, but genuine, and represent differences in the binding energetics, the interface contacts and the interactions between the protein and the solvent and solutes in it. Given the subtlety that clearly exists in the mechanism of binding for ligands in the active site of the cyclophilins and that this binding is “finessed” by the solution conditions, it is important to have characterisation of the binding in multiple solvents/solution conditions. This allows for a more comprehensive understanding of the molecular contacts and how solution changes are likely to alter the interaction between the protein and the ligand. For example, the relatively small energetic changes that arise from trapping water molecules at the binding interface (~ -0.05 kcal·mol⁻¹·K⁻¹ per trapped water) and/or the conformational subtlety in the contacts with this pseudo binding interface and ligands could potentially add up to 10s of nM difference in affinity, contributed from ΔC_p alone. In addition to these differences in the binding energetics/molecular contacts, understanding these solution differences potentially allows for specificity to be built into future ligand development by exploiting the differences in the way isoforms and the protein:ligand complexes interact with the solvent. To do this efficiently and rationally, we feel it is crucial to characterise the interaction as fully as possible, in multiple

solution environments that maintain physiological relevance.

The cyclophilins are validated drug targets for a number of diseases including HIV and HBV infection, malaria, recovery from ischemia, parasitic worm infection, immunosuppression and numerous proliferative cancers [23, 31-45]. Our laboratory is particularly interested in finding new compounds and analogues that could provide new chemical scaffolds for the synthesis of families of peptidomimetic molecules with potential isoform-specific inhibitory activity against these viral and parasite infections. Screening fragment (molecular weights in the 100 – 250 Da. range) libraries, either by high-throughput X-ray crystallography, NMR or SPR has been established as a rationale that allows rapid and effective interrogation of key binding interactions on the protein, reproducibly and specifically [66-68]. Even though a fragment's intrinsic potency is often very weak (K_d or IC_{50} values are typically in the high 100s of μM to mM ranges), the advantage is that they are small enough to minimize the chances of unfavourable molecular contacts that would prevent them from binding efficiently. This allows fragment libraries to be constructed to sample a large chemical diversity or target specific interactions on the protein. To this end we screened The Scottish Hit Discovery Facility (University of Dundee) fragment library on a surface of His-CypA created by our capture/stabilisation method. This fragment library represents a set (670 compounds) of diverse structures that comply with Astex's "Rule of Three" [66], have excellent medicinal chemistry tractability and feature as key pharmacophores in a large number of bioactives.

All the fragments were initially screened at 1 mM on a high-density (to account for the mass ratio of the fragments to His-CypA) surface of 2,866 RU covalently stabilized His-CypA and cyclophilin-A specific hits were further analysed with a 2-fold concentration series from 0.0625 mM to 1 mM (see materials and methods). We identified a fragment, 2,3-diaminopyridine that bound specifically and stoichiometrically to CypA. Typical sensorgrams showing the binding of this fragment to His-CypA are shown in Figure 5A with an average K_d of $248 \pm 60 \mu\text{M}$. We also solved the X-ray structure of this fragment bound to CypA to a resolution of 1.25 Å (PDB ID: 5LUD. Figure 5B – D; Table 2). As expected, the overall structure of CypA (Figure 5B & C) shows no major differences between the available apo and ligand bound structures of CypA (PDB IDs 2CPL and 4N1M, respectively). Electron density is present for only one copy of the ligand bound to the cyclophilin molecule (Figure 5C) in agreement with the stoichiometric binding determined from our SPR analysis (Figure 5A). The ligand is found bound within the small cleft, adjacent to the hydrophobic active site, commonly referred to as the Abu pocket (Figure 5B). The electron density for the ligand is excellent, with all of its atoms well defined allowing the unambiguous positioning of the ligand in the binding cleft (Figure 5C). The pyridine ring is sandwiched in the cleft formed by the main-chains of alanine-101 and asparagine-102 on one side, and the carbonyl of glycine-72 and the side-chain of glutamine-111 on the other. Only weak interactions are observed around the pyridine ring. Both amino groups point towards the back of the Abu pocket and somewhat surprisingly, only a single one – the 3-amino group – interacts directly with the protein; the 2-amino group forms a long range (3.31 Å) hydrogen-bond to the carbonyl of threonine-107 (Figure 5C). The strongest interactions that the ligand makes are to three water molecules (labeled w1 to w3; Figure 5C). These water molecules bridge interaction between the protein surface and the ligand. The 3-amino group forms a hydrogen-bond to a single water molecule (w3) which in turn bridges to the carbonyl of Threonine-73 (Figure 5C), whilst the 2-amino group forms hydrogen bonds to two water molecules (w1 and w2;

Figure 5C). These are very well defined with each having a low B-factor (17.64 and 17.67 Å², for w1 and w2, respectively) and are reported as being well conserved in a number of cyclophilin structures [15, 69]. They form an integral part of the interaction surface of the binding site of cyclophilins. Each of these water molecules form a further 3 hydrogen-bonds with the protein; w1 bonding to the main-chain carbonyls of threonine-107, glutamine-111 and the main-chain NH of glycine-107 (Figure 5C). w2 forms hydrogen-bonds to the carbonyl of Glycine-74 and the main-chain NHs of serine-110 and glutamine-111 (Figure 5C). The role of these well defined bridging waters reiterates that targeting water molecules rather than replacing them may in some case enhance or finesse the binding specificity and be preferable in considerations for ligand design [70, 71].

Recently a number of structures of sub-micromolar non-peptide inhibitors of cyclophilin-D (CypD), with evidence of inhibitory interactions with CypA, have been reported containing an aniline group bound within the Abu pocket [72]. Overlaying our CypA: 2,3-diaminopyridine structure reported here and the crystal structure of CypD in complex with one of these inhibitors (PDB ID: 4J5C) reveals a very close correlation between the aniline and the equivalent atoms of the 2,3-diaminopyridine (the mean distance for 7 equivalent atoms is 0.31, RMSD for 164 C-alpha protein atoms is 0.437, Figure 5D). It is noticeable that the amine group in the 4J5C structure does not have as tight an interaction to the equivalent w1 water molecule, compared to 2,3-diaminopyridine; the distance of the equivalent bond increasing by 0.34 Å to 3.53 Å. The amine group in the CypD structure is near equidistant between this water and the side-chain of arginine-124. The equivalent side-chain in CypA is lysine-82, and this residue side-chain adopts a different conformation that does not interact with the 2,3-diaminopyridine ligand (Figure 5D). This important difference provides a tantalising indication towards a route to isoform specific ligand design for CypA.

The structure of cyclophilin-A in complex with 2,3-diaminopyridine also validates our refined methodology for generating surface plasmon resonance sensor surfaces of recombinant his-tagged human cyclophilin-A. Furthermore, it highlights the potential role of bridging water molecules in ligand design and may provide insight for the future design of isoform specific cyclophilin inhibitors.

The new protocols reported here have very significantly, and rationally, optimised the basic methodology previously developed in our lab. This major protocol refinement has allowed for advancement in the biophysical characterisation of the protein and ligand binding interaction, and importantly, identification of a new non-peptide hit/ligand for CypA. The improved activity and stability of the material on the surface of the sensors, and the ability to use much lower concentrations of a complicated ligand with solubility issues (CsA), as a direct result of this increased sensitivity and activity, allowed the measurement of the binding interaction over a much wider temperature range, than has been possible before. We were able to expand the thermo-kinetic range by 10 °C in both directions in this new work - from 16 - 35 °C to 5 - 44 °C. This also enabled us to increase the data density across this expanded temperature range by a factor of nearly 3 (14 sets of kinetic measurements versus 5); resulting in a much more robust kinetic, affinity and thermodynamic characterisation of the binding interaction between CypA and CsA. Of note, the work presented here is the most comprehensive study of Cyp:CsA interaction by SPR to date, and was only achievable by the developments in methodology developed by our lab and described here.

Acknowledgments: This work was supported by Wellcome Trust Multi-User Equipment grant 101527/Z/13/Z, the Wellcome-UoE ISSF award (SEC-MALS equipment for the EPPF). We acknowledge Diamond Light Source (DLS) for time on I02 under proposal [7613].

Author contribution. MAW performed the purification, designed, performed and analysed the SPR and biophysical experiments and co-wrote the manuscript. MN designed the study, performed the fragment screening experiments and co-wrote the manuscript. EAB performed and analysed the DLS experiments and co-wrote the manuscript. IWM performed the data collection and X-ray crystallography experiments. MDW co-wrote the manuscript.

References.

1. Zeidan, E., Kopley, C. L., Sayes, C. & Sandros, M. G. (2015) Surface plasmon resonance: a label-free tool for cellular analysis, *Nanomedicine*. **10**, 1833-46.
2. Lee, T. H., Hirst, D. J. & Aguilar, M. I. (2015) New insights into the molecular mechanisms of biomembrane structural changes and interactions by optical biosensor technology, *Biochim Biophys Acta*. **1848**, 1868-85.
3. Nguyen, H. H., Park, J., Kang, S. & Kim, M. (2015) Surface plasmon resonance: a versatile technique for biosensor applications, *Sensors*. **15**, 10481-510.
4. Aristotelous, T., Hopkins, A. L. & Navratilova, I. (2015) Surface plasmon resonance analysis of seven-transmembrane receptors, *Methods Enzymol*. **556**, 499-525.
5. Wittenberg, N. J., Wootla, B., Jordan, L. R., Denic, A., Warrington, A. E., Oh, S. H. & Rodriguez, M. (2014) Applications of SPR for the characterization of molecules important in the pathogenesis and treatment of neurodegenerative diseases, *Expert review of neurotherapeutics*. **14**, 449-63.
6. Launay, H., Parent, B., Page, A., Hanouille, X. & Lippens, G. (2013) Dissociation kinetics of a binary complex in solution by protein displacement, *Angew Chem Int Ed Engl*. **52**, 12587-91.
7. Frostell, A., Vinterback, L. & Sjobom, H. (2013) Protein-Ligand Interactions Using SPR Systems, *Methods Mol Biol*. **1008**, 139-65.
8. Geschwindner, S., Carlsson, J. F. & Knecht, W. (2012) Application of optical biosensors in small-molecule screening activities, *Sensors*. **12**, 4311-23.
9. Bower, J. F. & Pannifer, A. (2012) Using fragment-based technologies to target protein-protein interactions, *Curr Pharm Des*. **18**, 4685-96.
10. Rich, R. L., Cannon, M. J., Jenkins, J., Pandian, P., Sundaram, S., Magyar, R., Brockman, J., Lambert, J. & Myszka, D. G. (2008) Extracting kinetic rate constants from surface plasmon resonance array systems, *Anal Biochem*. **373**, 112-20.
11. Navratilova, I., Papalia, G. A., Rich, R. L., Bedinger, D., Brophy, S., Condon, B., Deng, T., Emerick, A. W., Guan, H. W., Hayden, T., Heutmekers, T., Hoorelbeke, B., McCroskey, M. C., Murphy, M. M., Nakagawa, T., Parmeggiani, F., Qin, X., Rebe, S., Tomasevic, N., Tsang, T., Waddell, M. B., Zhang, F. F., Leavitt, S. & Myszka, D. G. (2007) Thermodynamic benchmark study using Biacore technology, *Anal Biochem*. **364**, 67-77.

12. Winzor, D. J. & Jackson, C. M. (2006) Interpretation of the temperature dependence of equilibrium and rate constants, *J Mol Recognit.* **19**, 389-407.
13. Branden, G., Sjogren, T., Schnecke, V. & Xue, Y. (2014) Structure-based ligand design to overcome CYP inhibition in drug discovery projects, *Drug Discov Today.*
14. Hughes, S. J., Millan, D. S., Kilty, I. C., Lewthwaite, R. A., Mathias, J. P., O'Reilly, M. A., Pannifer, A., Phelan, A., Stuhmeier, F., Baldock, D. A. & Brown, D. G. (2011) Fragment based discovery of a novel and selective PI3 kinase inhibitor, *Bioorg Med Chem Lett.* **21**, 6586-90.
15. Wear, M. A., Kan, D., Rabu, A. & Walkinshaw, M. D. (2007) Experimental determination of van der waals energies in a biological system, *Angew Chem Int Ed Engl.* **46**, 6453-6.
16. Anggayasti, W. L., Mancera, R. L., Bottomley, S. & Helmerhorst, E. (2016) Optimization of surface plasmon resonance experiments: Case of high mobility group box 1 (HMGB1) interactions, *Anal Biochem.* **499**, 43-50.
17. Helmerhorst, E., Chandler, D. J., Nussio, M. & Mamotte, C. D. (2012) Real-time and Label-free Bio-sensing of Molecular Interactions by Surface Plasmon Resonance: A Laboratory Medicine Perspective, *Clin Biochem Rev.* **33**, 161-73.
18. Schuck, P. & Zhao, H. (2010) The role of mass transport limitation and surface heterogeneity in the biophysical characterization of macromolecular binding processes by SPR biosensing, *Methods Mol Biol.* **627**, 15-54.
19. Rich, R. L. & Myszka, D. G. (2008) Survey of the year 2007 commercial optical biosensor literature, *J Mol Recognit.* **21**, 355-400.
20. Schumann, M., Jahreis, G., Kahlert, V., Lucke, C. & Fischer, G. (2011) Oligopeptide cyclophilin inhibitors: a reassessment, *Eur J Med Chem.* **46**, 5556-61.
21. Landrieu, I., Hanouille, X., Fritzinger, B., Horvath, D., Wieruszkeski, J. M. & Lippens, G. (2011) Ranking high affinity ligands of low solubility by NMR spectroscopy, *ACS Med Chem Lett.* **2**, 485-7.
22. Ludwig, C., Wear, M. A. & Walkinshaw, M. D. (2010) Streamlined, automated protocols for the production of milligram quantities of untagged recombinant human cyclophilin-A (hCypA) and untagged human proliferating cell nuclear antigen (hPCNA) using AKTExpress, *Protein Expr Purif.* **71**, 54-61.
23. Yang, Y., Moir, E., Kontopidis, G., Taylor, P., Wear, M. A., Malone, K., P., P. A., Turner, N. J. & Walkinshaw, M. D. (2007) Structure-based discovery of a family of synthetic cyclophilin inhibitors showing a cyclosporin-A phenotype in *C. elegans*, *Biochemical and Biophysical Research Communications.*
24. Fanghänel, J. & Fischer, G. (2003) Thermodynamic characterization of the interaction of human cyclophilin 18 with cyclosporin A, *Biophysical Chemistry.* **100**, 351-66
25. Wear, M. A. & Walkinshaw, M. D. (2006) Thermodynamics of the cyclophilin-A/cyclosporin-A interaction: a direct comparison of parameters determined by surface plasmon resonance using Biacore T100 and isothermal titration calorimetry, *Anal Biochem.* **359**, 285-7.
26. Wear, M. A., Patterson, A., Malone, K., Dunsmore, C., Turner, N. J. & Walkinshaw, M. D. (2005) A surface plasmon resonance-based assay for small molecule inhibitors of human cyclophilin A, *Anal Biochem.* **345**, 214-26.
27. Husi, H. & Zurini, M. G. (1994) Comparative binding studies of cyclophilins to cyclosporin A and derivatives by fluorescence measurements, *Anal Biochem.* **222**, 251-5.

28. Kofron, J. L., Kuzmic, P., Kishore, V., Colon-Bonilla, E. & Rich, D. H. (1991) Determination of kinetic constants for peptidyl prolyl cis-trans isomerases by an improved spectrophotometric assay, *Biochemistry*. **30**, 6127-34.
29. Liu, J., Albers, M. W., Chen, C. M., Schreiber, S. L. & Walsh, C. T. (1990) Cloning, expression, and purification of human cyclophilin in *Escherichia coli* and assessment of the catalytic role of cysteines by site-directed mutagenesis, *Proc Natl Acad Sci U S A*. **87**, 2304-8.
30. Handschumacher, R. E., Harding, M. W., Rice, J., Drugge, R. J. & Speicher, D. W. (1984) Cyclophilin: a specific cytosolic binding protein for cyclosporin A, *Science*. **226**, 544-7.
31. Galat, A. (2003) Peptidylprolyl cis/trans isomerases (immunophilins): biological diversity--targets--functions, *Curr Top Med Chem*. **3**, 1315-47.
32. Nigro, P., Pompilio, G. & Capogrossi, M. C. (2013) Cyclophilin A: a key player for human disease, *Cell death & disease*. **4**, e888.
33. Watashi, K., Ishii, N., Hijikata, M., Inoue, D., Murata, T., Miyanari, Y. & Shimotohno, K. (2005) Cyclophilin B is a functional regulator of hepatitis C virus RNA polymerase, *Mol Cell*. **19**, 111-22.
34. Franke, E. K. & Luban, J. (1995) Cyclophilin and gag in HIV-1 replication and pathogenesis, *Adv Exp Med Biol*. **374**, 217-28.
35. Franke, E. K. & Luban, J. (1996) Inhibition of HIV-1 replication by cyclosporine A or related compounds correlates with the ability to disrupt the Gag-cyclophilin A interaction, *Virology*. **222**, 279-82.
36. Franke, E. K., Yuan, H. E. & Luban, J. (1994) Specific incorporation of cyclophilin A into HIV-1 virions, *Nature*. **372**, 359-62.
37. Bose, S., Mathur, M., Bates, P., Joshi, N. & Banerjee, A. K. (2003) Requirement for cyclophilin A for the replication of vesicular stomatitis virus New Jersey serotype, *J Gen Virol*. **84**, 1687-99.
38. Liu, X., Sun, L., Yu, M., Wang, Z., Xu, C., Xue, Q., Zhang, K., Ye, X., Kitamura, Y. & Liu, W. (2009) Cyclophilin A interacts with influenza A virus M1 protein and impairs the early stage of the viral replication, *Cellular microbiology*. **11**, 730-41.
39. Theuerkorn, M., Fischer, G. & Schiene-Fischer, C. (2011) Prolyl cis/trans isomerase signalling pathways in cancer, *Curr Opin Pharmacol*. **11**, 281-7.
40. Gallay, P. A. (2012) Cyclophilin inhibitors: a novel class of promising host-targeting anti-HCV agents, *Immunol Res*. **52**, 200-10.
41. Lin, K. & Gallay, P. (2013) Curing a viral infection by targeting the host: the example of cyclophilin inhibitors, *Antiviral research*. **99**, 68-77.
42. Sherry, B., Yarlett, N., Strupp, A. & Cerami, A. (1992) Identification of cyclophilin as a proinflammatory secretory product of lipopolysaccharide-activated macrophages, *Proc Natl Acad Sci U S A*. **89**, 3511-5.
43. Obchoei, S., Weakley, S. M., Wongkham, S., Wongkham, C., Sawanyawisuth, K., Yao, Q. & Chen, C. (2011) Cyclophilin A enhances cell proliferation and tumor growth of liver fluke-associated cholangiocarcinoma, *Molecular cancer*. **10**, 102.

44. Obchoei, S., Wongkhan, S., Wongkham, C., Li, M., Yao, Q. & Chen, C. (2009) Cyclophilin A: potential functions and therapeutic target for human cancer, *Med Sci Monit.* **15**, RA221-32.
45. Baum, N., Schiene-Fischer, C., Frost, M., Schumann, M., Sabapathy, K., Ohlenschlager, O., Grosse, F. & Schlott, B. (2009) The prolyl cis/trans isomerase cyclophilin 18 interacts with the tumor suppressor p53 and modifies its functions in cell cycle regulation and apoptosis, *Oncogene.* **28**, 3915-25.
46. Naghibi, H., Tamura, A. & Sturtevant, J. M. (1995) Significant discrepancies between van't Hoff and calorimetric enthalpies, *Proc Natl Acad Sci U S A.* **92**, 5597-9.
47. Battye, T. G., Kontogiannis, L., Johnson, O., Powell, H. R. & Leslie, A. G. (2011) iMOSFLM: a new graphical interface for diffraction-image processing with MOSFLM, *Acta Crystallogr D Biol Crystallogr.* **67**, 271-81.
48. Evans, P. R. & Murshudov, G. N. (2013) How good are my data and what is the resolution?, *Acta Crystallogr D Biol Crystallogr.* **69**, 1204-14.
49. Murshudov, G. N., Skubak, P., Lebedev, A. A., Pannu, N. S., Steiner, R. A., Nicholls, R. A., Winn, M. D., Long, F. & Vagin, A. A. (2011) REFMAC5 for the refinement of macromolecular crystal structures, *Acta Crystallogr D Biol Crystallogr.* **67**, 355-67.
50. Winn, M. D., Ballard, C. C., Cowtan, K. D., Dodson, E. J., Emsley, P., Evans, P. R., Keegan, R. M., Krissinel, E. B., Leslie, A. G., McCoy, A., McNicholas, S. J., Murshudov, G. N., Pannu, N. S., Potterton, E. A., Powell, H. R., Read, R. J., Vagin, A. & Wilson, K. S. (2011) Overview of the CCP4 suite and current developments, *Acta Crystallogr D Biol Crystallogr.* **67**, 235-42.
51. Emsley, P., Lohkamp, B., Scott, W. G. & Cowtan, K. (2010) Features and development of Coot, *Acta Crystallogr D Biol Crystallogr.* **66**, 486-501.
52. Wear, M. A. & Walkinshaw, M. D. (2007) Determination of the rate constants for the FK506 binding protein/rapamycin interaction using surface plasmon resonance: an alternative sensor surface for Ni²⁺-nitrilotriacetic acid immobilization of His-tagged proteins, *Anal Biochem.* **371**, 250-2.
53. Nieba, L., Nieba-Axmann, S. E., Persson, A., Hamalainen, M., Edebratt, F., Hansson, A., Lidholm, J., Magnusson, K., Karlsson, A. F. & Pluckthun, A. (1997) BIACORE analysis of histidine-tagged proteins using a chelating NTA sensor chip, *Anal Biochem.* **252**, 217-28.
54. Chu, R., Reczek, D. & Brondyk, W. (2014) Capture-stabilize approach for membrane protein SPR assays, *Sci Rep.* **4**, 7360.
55. Kimple, A. J., Muller, R. E., Siderovski, D. P. & Willard, F. S. (2010) A capture coupling method for the covalent immobilization of hexahistidine tagged proteins for surface plasmon resonance, *Methods Mol Biol.* **627**, 91-100.
56. Kallen, J., Spitzfaden, C., Zurini, M. G., Wider, G., Widmer, H., Wuthrich, K. & Walkinshaw, M. D. (1991) Structure of human cyclophilin and its binding site for cyclosporin A determined by X-ray crystallography and NMR spectroscopy, *Nature.* **353**, 276-9.
57. Fanghanel, J. & Fischer, G. (2003) Thermodynamic characterization of the interaction of human cyclophilin 18 with cyclosporin A, *Biophys Chem.* **100**, 351-66.

58. Chen, S., Zhao, X., Tan, J., Lu, H., Qi, Z., Huang, Q., Zeng, X., Zhang, M., Jiang, S., Jiang, H. & Yu, L. (2007) Structure-based identification of small molecule compounds targeting cell cyclophilin A with anti-HIV-1 activity, *Eur J Pharmacol.* **565**, 54-9.
59. Li, J., Chen, J., Gui, C., Zhang, L., Qin, Y., Xu, Q., Zhang, J., Liu, H., Shen, X. & Jiang, H. (2006) Discovering novel chemical inhibitors of human cyclophilin A: virtual screening, synthesis, and bioassay, *Bioorg Med Chem.* **14**, 2209-24.
60. Li, J., Chen, J., Zhang, L., Wang, F., Gui, C., Zhang, L., Qin, Y., Xu, Q., Liu, H., Nan, F., Shen, J., Bai, D., Chen, K., Shen, X. & Jiang, H. (2006) One novel quinoxaline derivative as a potent human cyclophilin A inhibitor shows highly inhibitory activity against mouse spleen cell proliferation, *Bioorg Med Chem.* **14**, 5527-34.
61. Guo, H. X., Wang, F., Yu, K. Q., Chen, J., Bai, D. L., Chen, K. X., Shen, X. & Jiang, H. L. (2005) Novel cyclophilin D inhibitors derived from quinoxaline exhibit highly inhibitory activity against rat mitochondrial swelling and Ca²⁺ uptake/ release, *Acta Pharmacol Sin.* **26**, 1201-11.
62. Mikol, V., Kallen, J., Pflugl, G. & Walkinshaw, M. D. (1993) X-ray structure of a monomeric cyclophilin A-cyclosporin A crystal complex at 2.1 Å resolution, *J Mol Biol.* **234**, 1119-30.
63. Altschuh, D., Braun, W., Kallen, J., Mikol, V., Spitzfaden, C., Thierry, J. C., Vix, O., Walkinshaw, M. D. & Wuthrich, K. (1994) Conformational polymorphism of cyclosporin A, *Structure.* **2**, 963-72.
64. Kallen, J., Mikol, V., Taylor, P. & Walkinshaw, M. D. (1998) X-ray structures and analysis of 11 cyclosporin derivatives complexed with cyclophilin A, *J Mol Biol.* **283**, 435-49.
65. Holdgate, G. A., Tunnicliffe, A., Ward, W. H., Weston, S. A., Rosenbrock, G., Barth, P. T., Taylor, I. W., Pauptit, R. A. & Timms, D. (1997) The entropic penalty of ordered water accounts for weaker binding of the antibiotic novobiocin to a resistant mutant of DNA gyrase: a thermodynamic and crystallographic study, *Biochemistry.* **36**, 9663-73.
66. Congreve, M., Carr, R., Murray, C. & Jhoti, H. (2003) A 'rule of three' for fragment-based lead discovery?, *Drug Discov Today.* **8**, 876-7.
67. Blundell, T. L., Jhoti, H. & Abell, C. (2002) High-throughput crystallography for lead discovery in drug design, *Nat Rev Drug Discov.* **1**, 45-54.
68. Carr, R. & Jhoti, H. (2002) Structure-based screening of low-affinity compounds, *Drug Discov Today.* **7**, 522-7.
69. Mikol, V., Papageorgiou, C. & Borer, X. (1995) The role of water molecules in the structure-based design of (5-hydroxynorvaline)-2-cyclosporin: synthesis, biological activity, and crystallographic analysis with cyclophilin A, *J Med Chem.* **38**, 3361-7.
70. Garcia-Sosa, A. T. (2013) Hydration properties of ligands and drugs in protein binding sites: tightly-bound, bridging water molecules and their effects and consequences on molecular design strategies, *J Chem Inf Model.* **53**, 1388-405.
71. Garcia-Sosa, A. T. & Mancera, R. L. (2010) Free Energy Calculations of Mutations Involving a Tightly Bound Water Molecule and Ligand Substitutions in a Ligand-Protein Complex, *Mol Inform.* **29**, 589-600.
72. Ahmed-Belkacem, A., Colliandre, L., Ahnou, N., Nevers, Q., Gelin, M., Bessin, Y., Brillet, R., Cala, O., Douguet, D., Bourguet, W., Krimm, I., Pawlowsky, J. M. & Guichou, J. F. (2016) Fragment-based discovery of a

new family of non-peptidic small-molecule cyclophilin inhibitors with potent antiviral activities, *Nat Commun.* **7**, 12777.

Tables and figure legends

Temp (°C)	K_d (nM)	k_a ($\mu\text{M}^{-1}\cdot\text{s}^{-1}$)	k_d ($\times 10^{-3} \text{ s}^{-1}$)	
5	5.5 ± 1.2	0.22 ± 0.05	1.2 ± 0.08	
8	7.1 ± 1.2	0.27 ± 0.02	1.9 ± 0.2	
11	7.6 ± 1.7	0.33 ± 0.08	2.5 ± 0.1	
14	9.6 ± 1.2	0.42 ± 0.04	4.1 ± 0.2	
17	12.2 ± 2.1	0.47 ± 0.08	5.7 ± 0.2	
20	14.3 ± 1.4	0.59 ± 0.04	8.4 ± 0.4	
23	20.4 ± 2.7	0.61 ± 0.1	12.4 ± 0.6	
26	27.6 ± 4.9	0.67 ± 0.1	18.5 ± 1	
29	38.4 ± 8.2	0.77 ± 0.14	29.5 ± 2.1	
32	52 ± 6.1	0.83 ± 0.09	43.0 ± 1.0	
35	75.1 ± 13	1.1 ± 0.21	83.6 ± 3.4	
38	90.1 ± 9.6	1.3 ± 0.36	118 ± 3.6	
41	117 ± 16.6	1.8 ± 0.41	211 ± 7.8	
<i>van't Hoff analysis</i>				
Temp (°C)	ΔG° (kcal·mol ⁻¹)	ΔH° (kcal·mol ⁻¹)	$T\Delta S^\circ$ (kcal·mol ⁻¹)	ΔC_p (kcal·mol ⁻¹ ·K ⁻¹)
25 °C	- 10.38 ± 0.21	- 15. 50 ± 0.8	- 5.12 ± 0.5	- 0.41 ± 0.16

Table 1. Temperature dependence of the kinetic and equilibrium affinity constants for CsA binding to recombinant human His-CypA, determined by Biacore™ T200. K_d values (mean ± SE, n = 3) were calculated using the formula $K_d = k_d / k_a$. van't Hoff parameters calculated from a fit of equation 4 to a plot of $\ln K_d$ versus $1/T$ in K (Figure 3).

X-ray Source	I02 (DLS)
Wavelength (Å)	0.97949
Space group	$P2_12_12_1$
Unit cell (Å)	$a = 42.53, b = 54.48, c = 86.81$
Resolution range (Å)	33.95–1.25 (1.27–1.25)
Total observations	203449
Unique reflections ^a	55267 (2453)
Redundancy	3.7 (2.7)
$I/\sigma(I)$ ^a	8.7 (1.0)
R_{merge} (%) ^a	6.5 (59.4)
Completeness (%) ^a	97.8 (89.5)
Refinement statistics	
Resolution limit (Å) ^a	33.0–1.25 (1.28–1.25)
R -factor (%)	19.3 (31.4)
R_{free} (%)	21.9 (32.2)
No. of protein atoms	1303
No. of water atoms	238
No. of ligand atoms	8
RMSD bond lengths (Å)	0.0254
RMSD bond angles (°)	2.294
Mean B factor (Å ²)	17.751

^aValues in parentheses refer to the highest-resolution shell.

Table 2. X-ray data collection and refinement statistics.

Figure legends.

Figure 1. (A) Ultra-pure, monodisperse and highly active protein is used for sensor-surface generation. (A) 4 – 15 % acrylamide SDS Stain-free TGX gel (BioRad) illustrating the final purity of His-CypA (2 μg total protein). Standards are shown to the left. **(B)** Size-exclusion chromatography (ÅKTA-Micro; GE Healthcare) coupled to UV, static light scattering and refractive index detection (Viscotec SEC-MALS 20 and Viscotek RI Detector:VE3580; Malvern Instruments), were used to determine the molar mass of His-CypA in solution. 100 μL of 1 $\text{mg}\cdot\text{mL}^{-1}$ His-CypA was run on a Superdex-75 10/300 GL (GE Healthcare) size exclusion column pre-equilibrated in 10 mM NaH_2PO_4 , pH 7.5; 150 mM NaCl at 22 $^\circ\text{C}$, at 0.8 $\text{ml}\cdot\text{min}^{-1}$. Light scattering, refractive index (RI) and $A_{280\text{nm}}$ were analysed by a homo-polymer model (OmniSEC software, v 5.1; Malvern Instruments) using the following parameters: $\partial A / \partial c$ at 280nm 0.71 $\text{AU}\cdot\text{mL}\cdot\text{mg}^{-1}$ and $\partial n / \partial c$ of 0.185 $\text{mL}\cdot\text{g}^{-1}$. His-CypA protein elutes a single sharp peak with a correlative R_s of 1.82 ± 0.1 nm (mean \pm SEM, $n = 5$). Elution positions for standards are shown above the chromatograph. The molar mass average across the elution profile is 19.8 kDa. with excellent mono-dispersity ($M_w/M_n = 1.003$). The theoretical molecular weight of His-CypA is 21.04 kDa. DLS analysis (data not shown) also indicates high mono-dispersity for His-CypA solutions with a mean R_h of 1.85 ± 0.17 nm (mean \pm SEM, $n = 5$), a polydispersity index of ≤ 0.1 , and a correlative molecular weight of between 19 to 21 kDa, consistent with a highly pure and monomeric protein solution. **(C)** Inhibition of His-CypA's PPIase activity by CsA. Initial background corrected reaction (V_o) rate in $\mu\text{M}\cdot\text{s}^{-1}$ is plotted *versus* the concentration of CsA in nM. Solid lines are a least squares fit of the data to equation 1 (see Materials and Methods). Each point is the mean \pm SE, $n = 3$. The mean K_i value for CsA, at 12 $^\circ\text{C}$, is 15.03 ± 1.38 nM.

Figure 2. Optimisation of capture/stabilization parameters on modified NTA-sensor surfaces. (A) Graphical representation comparing the EDC:NHS activation time with the final levels of immobilized His-CypA (white bars, left axis) and the corresponding specific activity of the surfaces (dark gray bars, right axis). Contact time in each experiment was 30 secs with a 100 nM solution of His-CypA. In all cases the experimental RU_{max} value was generated by passing 1.2 μM CsA in 10 mM NaH_2PO_4 , pH 7.5, 150 mM NaCl, 50 μM EDTA; 0.05 % surfactant P20; 1 % ethanol over the surface. **(B)** Representative reference corrected SPR sensorgrams (black), monitored on a surface with 612 RU of covalently stabilized His-CypA (100 nM, 30 s contact following 180 s activation). A 2-fold dilution series of CsA, from 500 nM - 1.95 nM, was run at 25 $^\circ\text{C}$ in 10 mM NaH_2PO_4 , pH 7.5, 150 mM NaCl, 1 mM EDTA; 0.05 % surfactant P20; 1 % ethanol at 100 $\mu\text{l}\cdot\text{min}^{-1}$. The on- and off-rate constants were by globally fitting (red) a 1:1 kinetic binding model to the sensorgrams using the analysis software (v2.02, GE Healthcare) supplied with the instrument. Mean values ($n = 5$, \pm SEM) determined for the on-rate (k_a), off-rate (k_d) and equilibrium dissociation constants (K_d) are 0.79 ± 0.06 $\mu\text{M}^{-1}\cdot\text{s}^{-1}$, 0.018 ± 0.004 s^{-1} and 22.8 ± 3.6 nM, respectively. **(C)** Reference corrected SPR single cycle kinetic sensorgrams (black), monitored on a surface with 58 RU of covalently stabilized His-CypA (10 nM, 30 s contact following 180 s activation). A 3-fold dilution series of CsA, from 200 nM - 2.46 nM, was run at 25 $^\circ\text{C}$ in 10 mM NaH_2PO_4 , pH 7.5, 150 mM NaCl, 1 mM EDTA; 0.05 % surfactant P20; 1 % ethanol at 100 $\mu\text{l}\cdot\text{min}^{-1}$. The on- and off-rate constants were by globally fitting (red) a 1:1 kinetic binding model to

the sensorgrams using the analysis software (v2.02, GE Healthcare) supplied with the instrument. Mean values ($n = 3$, \pm SEM) determined for the on-rate (k_a), off-rate (k_d) and equilibrium dissociation constants (K_d) are $0.73 \pm 0.07 \mu\text{M}^{-1}\cdot\text{s}^{-1}$, $0.018 \pm 0.006 \text{ s}^{-1}$ and $24.7 \pm 5.3 \text{ nM}$, respectively. **(D)** Reference corrected SPR single cycle kinetic sensorgrams (black), monitored on a surface with 780 RU of His-CypA immobilized utilizing standard amine coupling chemistry ($100 \mu\text{g}\cdot\text{ml}^{-1}$ His-CypA in 10 mM acetate, pH 5.8, with a 30 second contact time with the activated surface). A 3-fold dilution series of CsA, from 200 nM - 2.46 nM, was run at 25°C in 10 mM NaH_2PO_4 , pH 7.5, 150 mM NaCl, 1 mM EDTA; 0.05 % surfactant P20; 1 % ethanol at $100 \mu\text{l}\cdot\text{min}^{-1}$. The on- and off-rate constants were by globally fitting (red) a 1:1 kinetic binding model to the sensorgrams using the analysis software (v2.02, GE Healthcare) supplied with the instrument. Mean values ($n = 3$, \pm SEM) determined for the on-rate (k_a), off-rate (k_d) and equilibrium dissociation constants (K_d) are $0.48 \pm 0.1 \mu\text{M}^{-1}\cdot\text{s}^{-1}$, $0.14 \pm 0.1 \text{ s}^{-1}$ and $291.7 \pm 104 \text{ nM}$, respectively.

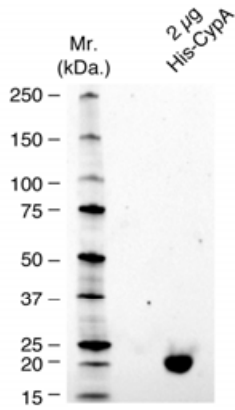
Figure 3. Effect of temperature on the binding of CsA to His-CypA. Reference corrected SPR single cycle kinetic sensorgrams (black), monitored on a surface with 2,378 RU of covalently stabilized His-CypA (250 nM, 30 s contact following 180 s activation) for the indicated CsA concentrations (200 nM - 2.46 nM) from 5 °C to 44 °C in 3 °C increments. The on- and off-rate constants were by globally fitting (red) a 1:1 kinetic binding model to the sensorgrams using the analysis software (v2.02, GE Healthcare) supplied with the instrument. Mean values ($n = 3$, \pm SEM) determined for the on-rate (k_a), off-rate (k_d) and equilibrium dissociation constants (K_d) are shown in Table 1.

Figure 4. Thermodynamic characterisation of the CypA:CsA interaction by SPR Biacore™ T200. Plot of $\ln K_d$ versus $1/T$ in K. Data was fit (solid line) to Equation 4 using Kaleidagraph v4.1.3 software (Synergy Software, Reading, PA). Thermodynamic parameters calculated from this data are shown in Table 1

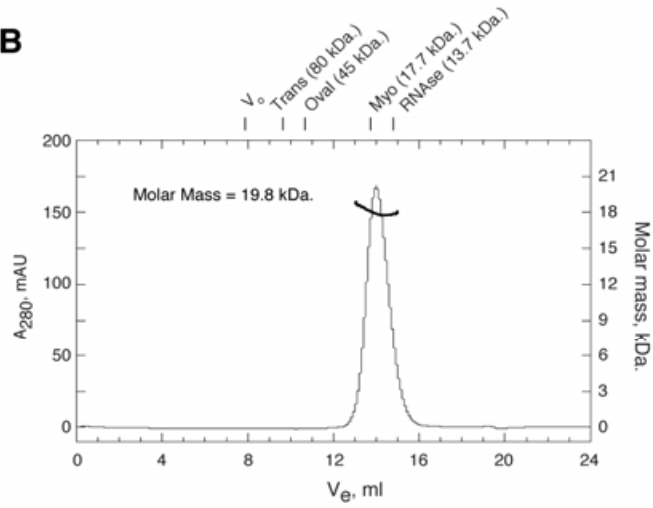
Figure 5. Binding and structural analysis of His-CypA:2,3-diaminopyridine complex. **(A)** Reference corrected SPR single cycle kinetic sensorgrams (black), monitored on a surface with 2,866 RU of covalently stabilized His-CypA (300 nM, 30 s contact following 180 s activation) for the indicated 2,3-diaminopyridine concentrations (1 mM – 62.5 μM). The apparent equilibrium dissociation was determined by fitting (red) a 1:1 Langmuir binding model (inset) to the sensorgrams using the analysis software (v2.02, GE Healthcare) supplied with the instrument. The mean K_d value is $248 \pm 60 \mu\text{M}$ ($n = 3$, \pm SEM). **(B)** Electrostatic surface of the structure of CypA in complex with 2,3-diaminopyridine (PDB ID: 5LUD). The ligand is drawn with purple carbons and is observed in the Abu pocket, the hydrophobic active site is below in the orientation shown. **(C)** Electron density and 2,3-diaminopyridine:CypA interaction details. The omit electron density ($F_o - F_c$) contoured at 3σ is shown around the 2,3-diaminopyridine ligand as a green mesh, all ligand atoms are clearly defined in density. Direct hydrogen bond interactions to the ligand are represented as yellow dashes, whilst bridged water-protein hydrogen bonds are represented as black dashes. **(D)** Comparison of the CypA:2,3-diaminopyridine structure (grey carbons - protein, purple carbons - ligand) and the CypD:ligand structure of 4J5C (Cyan carbons – protein, Green carbons – ligand). Comparative distances in the respective complexes are indicated (yellow dashes/black labels, CypA:2,3-diaminopyridine; red dashes/red

labels CypD:ligand structure 4J5C).

A



B



C

